Hindawi
Journal of Function Spaces
Volume 2023, Article ID 9851623, 1 page
https://doi.org/10.1155/2023/9851623

Retraction

Retracted: InSAR Phase Unwrapping Algorithm Based on Deep GAN

Journal of Function Spaces

Received 12 December 2023; Accepted 12 December 2023; Published 13 December 2023

This article has been retracted by Hindawi, as publisher, following an investigation undertaken by the publisher [1]. This investigation has uncovered evidence of systematic manipulation of the publication and peer-review process. We cannot, therefore, vouch for the reliability or integrity of this article.

Please note that this notice is intended solely to alert readers that the peer-review process of this article has been compromised.

Wiley and Hindawi regret that the usual quality checks did not identify these issues before publication and have since put additional measures in place to safeguard research integrity.

We wish to credit our Research Integrity and Research Publishing teams and anonymous and named external researchers and research integrity experts for contributing to this investigation.

The corresponding author, as the representative of all authors, has been given the opportunity to register their agreement or disagreement to this retraction. We have kept a record of any response received.

References

[1] C. Wang, P. Sun, Z. Li, and L. Tang, "InSAR Phase Unwrapping Algorithm Based on Deep GAN," *Journal of Function Spaces*, vol. 2023, Article ID 9230780, 11 pages, 2023.

Hindawi
Journal of Function Spaces
Volume 2023, Article ID 9230780, 11 pages
https://doi.org/10.1155/2023/9230780

Research Article

InSAR Phase Unwrapping Algorithm Based on Deep GAN

Chenxia Wang,[1] **Pingli Sun**,[1] **Zheng Li**,[1] **and Linlin Tang**[2]

[1]*Department of Education and Teaching, Zhengzhou Preschool Education College, Zhengzhou, Henan 450000, China*
[2]*School of Computer Science and Technology, Harbin Institute of Technology, Shenzhen, Guangdong 518055, China*

Correspondence should be addressed to Chenxia Wang; 2003003@zzpec.edu.cn

Received 26 July 2022; Revised 13 September 2022; Accepted 23 September 2022; Published 27 March 2023

Academic Editor: Miaochao Chen

At present, the traditional phase unwrapping algorithm is difficult to balance the accuracy and unwrapping efficiency. The traditional phase unwrapping algorithm is difficult to balance the accuracy and efficiency in the phase unwrapping experiments of simulated and measured topographic interferograms. In this paper, the phase unwrapping technology will be studied under the framework of deep learning theory according to the development trend of InSAR intelligence. A phase unwrapping algorithm based on deep GAN is proposed. The model structure includes dense convolution layer blocks and series structure, so that the network can achieve a better balance between feature extraction and detail preservation of interferogram. This is helpful to improve the phase unwrapping accuracy and training efficiency of the network. The experimental results show that the algorithm has a good expansion effect on the interferogram with high signal-to-noise ratio. The synthesis algorithm makes full use of the advantages of the branch cutting method and the finite element method. The phase reliable region and unreliable region are determined, and the transmission of phase error from the unreliable region to reliable region is effectively avoided. The accuracy of the phase unwrapping results in the reliable region is ensured, and the overall phase unwrapping convergence accuracy is greatly improved.

1. Introduction

Since the 1950s, the theory and technology of synthetic aperture radar remote sensing have been in a state of rapid development. Compared with traditional visible light or infrared remote sensing technology, SAR has all-weather and all-day observation capabilities [1]. It does not rely on sunlight as an illumination source and can penetrate clouds, mist, and dust [2]. Now, it has gradually become an important object. Interferometric synthetic aperture radar is a remote sensing mapping technology that combines synthetic aperture radar and radio astronomy interferometry [3]. In the past few decades, InSAR theory and technology have been continuously developed. InSAR mainly uses the phase information of two or more SAR images to obtain target elevation and has been widely used in geographic information system construction, environmental monitoring, and surface deformation monitoring, seismic activity, volcanic activity, and other fields [4]. Interferogram phase unwrapping is a key step in InSAR elevation measurement technology, which directly affects the accuracy of InSAR elevation measurement [5].

At present, there are many research achievements in SAR image segmentation processing technology. However, due to the complexity of SAR terrain scene, all kinds of segmentation algorithms have great pertinence and poor universality. This paper summarizes these research results, summarizes the existing segmentation methods, and segments the SAR image according to the characteristics of using prior knowledge. Methods are mainly divided into two categories: data-driven and model-driven. SAR image segmentation based on data-driven directly operates on the current image data. Although it also uses the prior knowledge, it does not depend on the prior knowledge. Model-driven SAR image segmentation is directly based on prior knowledge. In addition, the performance evaluation index of SAR image segmentation algorithm is given. And use Radarsat data to verify the performance of the above segmentation algorithm. Deep learning (DL) is a machine learning method that simulates the neural structure of the

human brain, and it is also a breakthrough technology in the field of computer vision for decades. It can effectively extract rich low-level and high-level feature information from sample data. It has achieved the best performance in many problems in different fields, such as speech recognition, text data mining, text translation, face recognition, image classification and recognition, image segmentation, etc [6]. With the expansion of the application of DL technology by domestic and foreign scholars, it has been gradually applied to synthetic aperture radar (SAR) image classification and segmentation, SAR target detection, interferometric SAR image segmentation, SAR image registration, and inverse synthetic aperture radar (ISAR) imaging. InSAR interferogram phase unwrapping and other fields effectively promote the development of related technologies in these fields [7, 8].

This paper analyzes the phase unwrapping problem in synthetic aperture radar interferometry. The study is divided into five parts. The first section describes the phase unwrapping algorithm based on full convolution and the improved U-net phase unwrapping algorithm. This paper proposes to use the above expansion algorithm to study the interferometric SAR interferogram data set. Section 2 describes the history and current situation of phase unwrapping algorithm and deep learning. The importance of phase unwrapping derived from InSAR height measurement principle is introduced. Section 3 analyzes the technical principle of InSAR and the basic theory of GAN. The traditional phase unwrapping algorithm is studied. Three classical GAN neural networks used in phase unwrapping are introduced. The model architecture is introduced and analyzed in detail. Section 4 simulates the experimental analysis of interferogram. Finally, an improved U-net phase unwrapping algorithm is proposed, and the model structure is divided into modules. Compared with the deep learning phase unwrapping algorithm, the unwrapping results of the proposed algorithm are analyzed.

2. State of the Art

2.1. Phase Unwrapping Algorithm Research History and Present. Phase unwrapping is an important step in InSAR data, and its results directly affect the accuracy of target elevation measurements. At present, phase unwrapping algorithms are mainly divided into three categories, including path-tracking algorithms represented by branch-cut and quality-guided algorithms, minimum-norm algorithms represented by least squares, and state-of-the-art algorithms represented by Kalman filtering [9]:

(1) Path tracking algorithms use various strategies to define a suitable path and integrate along this path to obtain its unwrapped phase to minimize or avoid the cumulative effect of errors in the phase unwrapping process, including the classic branch proposed by Kumar et al. [10]. In recent years, the tangent method, which detects the residue points and places the branch tangents according to the polarity balance rule, effectively avoids the transmission of unwrapping errors [11]. If the residue points are too dense, it will lead to an "island" effect in the unwrapping results. The quality map-guided method uses the precomputed quality map as auxiliary information to make the phase unwrapping proceed in the direction of high-quality pixels to low-quality pixels; Flynn equals the mask-cut method proposed in 1996. This algorithm combines the advantages of the branch-cut method and the quality-map-guided algorithm and uses the quality map to guide the placement of branch tangents. Tang et al. improved the quality of graph-guided method by combining the minimum discontinuity method to shorten the running time of the algorithm [12]

(2) The state estimation algorithm transforms the interferogram phase unwrapping problem into a state estimation problem under nonlinear conditions and performs phase noise suppression and phase unwrapping almost simultaneously [13]. These include the phase unwrapping algorithm improved by using the extended Kalman filter model in 2008, which has better unwrapping results; the unscented Kalman filter phase unwrapping algorithm proposed by Y et al. and a series of nonlinear filter phase unwrapping algorithms The unwrapping algorithm optimizes the performance of the algorithm by combining the gradient estimator and the fast path tracking strategy to ensure the accuracy and speed of the unwrapping. Then, on this basis, the particle filter phase unwrapping algorithm and the information filter phase unwrapping algorithm are proposed [14]

2.2. History and Current Situation of Deep Learning Research. The concept of deep learning originates from artificial neural network, which is a technology for feature learning on a large amount of data. Its essence is a deep neural network that simulates the human brain for learning and judgment. The convolutional neural network LeNet-5 by combining the convolutional layer and the downsampling layer, which can realize the task of handwritten digit recognition, and this network became the pioneer of the modern structure of the convolutional neural network (CNN). Since then, Li et al. took the lead in using the nonlinear activation function and the Dropout method to prevent overfitting and proposed a new CNN structure AlexNet based on the LeNt-5 model [15]. This network has become an important turning point in the development of deep learning and has paved the way for in-depth research on convolutional neural networks; in 2019, Ma and Li proposed VGGNet, which improves the overall performance of the network by increasing the number of layers of the model [16]. The VGG16 and VGG19 convolutional neural networks have been successfully constructed [17]. Compared with the previous network structure, the error rate of VGGNet in the classification task is greatly reduced. The concept of deep learning originates from artificial neural networks and is a feature learning technology for large amounts of data [18]. The essence is a deep neural network that simulates the human brain for learning and judgment [19]. Since then, J et al took the lead in using

the nonlinear activation function ReLu and Dropout method to prevent overfitting and proposed a new CNN structure AlexNet based on the LeNt-5 model. This network has become an important turning point in the development of deep learning and has paved the way for in-depth research on convolutional neural networks; which improves the overall performance of the network by increasing the number of layers of the model. The VGG16 and VGG19 convolutional neural networks were successfully constructed. Compared with the previous network structure, the error rate of VGGNet in the classification task was greatly reduced [20].

In addition, GAN neural network has gradually begun to be applied to the field of interferogram phase disentanglement. This method transforms the interferogram phase unwrapping problem into a multiclassification problem. The VGG16 network model is used in the first half of the network model to downsample the input image, and the convolutional layer is used instead of the fully connected layer. The feature map enters the decoding path after going through the convolution layer and the pooling layer, and finally, the feature map is upsampled and the classification result is output. Based on the DeeplabV3+ network, the algorithm similarly transforms the unwrapping problem into the classification problem of phase ambiguities and divides, stacks, and corrects the interferogram. After processing, better disentanglement results can be obtained. After the winding phase interferogram is passed through the trained network, the unwrapped phase interferogram can be directly obtained. The network establishes the relationship between the winding phase and the real. The nonlinear mapping relationship between the phases has a good unwrapping effect.

3. Methodology

3.1. InSAR Technology Principle

3.1.1. InSAR Elevation Measurement Principle. The basic idea of InSAR technology is to use two antennas installed on the same flight carrier to observe the same target and obtain the complex radar image pair of the target area. The digital elevation model (DEM) of the target area is reconstructed by calculating the digital elevation information of the target point by calculating the phase information difference contained in the pixels in the two interferograms (i.e., the main and auxiliary images of the interference pair). InSAR error propagation can be used for three-dimensional surface reconstruction by using the phase data of primary differential interference and satellite orbit data. The surface deformation can be detected by the second differential interference processing. This interference analysis needs to use radar system parameters, radar platform attitude (baseline) data phase observation, terrain data (used for terrain phase deduction in secondary difference), etc. Obviously, the uncertainty or error of these data will propagate to the interference elevation or deformation results. This section will introduce the area elevation calculation method through the geometric schematic diagram of InSAR elevation measurement.

In Figure 1, Ai and A2 represent radar satellite antennas; assuming that the distance between the two antennas is the baseline length of B, the horizontal angle of the baseline is a, and the downward viewing angle of the antenna A1 relative to point P is day. The height of the radar antenna A1 is H. P is a point in the observation area; the distances from the two radar satellite antennas AI and A2 to the observation point P are R1 and R2, respectively; and the height of the observation point P from the ground is h. Due to the difference in the viewing angles of the antennas A1 and A2, the two images cannot be completely overlapped. In order to make the pixels in the two images correspond to each other, an image registration operation is required. Assuming that the signals received by the antennas An and A2 are S1 and S2, respectively, the following formula is the complex conjugate operation of the registered image:

$$S_1 \times S_2{}^* = A \exp\left[j\frac{4\pi}{\lambda}(R_2 - R_1)\right]. \tag{1}$$

Among them, "$*$" is the conjugate symbol, A is the amplitude of the signal, and 2 is the wavelength of the radar. From this, the phase difference of the two SAR images can be obtained:

$$\varphi = \varphi_2 - \varphi_1 = \frac{4\pi}{\lambda}(R_2 - R_1). \tag{2}$$

According to the cosine law,

$$R_2^2 = R_1^2 + B^2 - 2R_1 B\cos\left(\frac{\pi}{2} - \theta + \alpha\right). \tag{3}$$

The height of the observation point P is derived from the above formula:

$$h = H - R_1 \sin\alpha - \sec\left(\frac{-\lambda\phi}{4\pi B}\right). \tag{4}$$

In formula (4), H, R_1, and a are all known quantities, so the above formula is only related to the real phase φ. Since the range of the main phase value limited by the trigonometric function operation is between $[-\pi, n)$, $2k\pi k = 0, 1, 2\cdots$:

$$\phi = \varphi + \phi_c = \varphi + 2k\pi \quad (k = 0, \pm 1, \pm 2, \cdots). \tag{5}$$

The k in equation (5) is called the phase ambiguity number, which can be classified to obtain the phase ambiguity number distribution map in the deep learning phase unwrapping. The main value of the phase is the winding phase. The process of recovering the real phase of the interferogram from the winding phase is phase unwrapping. Only by obtaining the real phase can the observation target elevation be obtained. It can be seen that phase unwrapping is an important step in the InSAR elevation measurement link.

3.1.2. InSAR Interferometric Phase Extraction Process of Surface Elevation Information. InSAR applications mainly

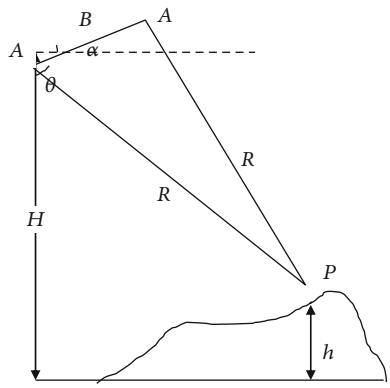

Figure 1: InSAR geometric schematic diagram.

include surface deformation measurement and 3D reconstruction, including the following steps:

Interferometric image pair prefiltering and image pair registration processing: during the actual measurement process, the interferogram will be spectral shifts that occur in both the range and azimuth directions, resulting in phase noise in the interference image pair. Therefore, the interferogram needs to be prefiltered to improve the coherence of the interferogram. The topography is more sensitive to the influence of the phase. If the corresponding pixels of the two images are deviated, it will cause a large error in the measurement results. Therefore, it is necessary to perform registration processing on the interference image pair. The registered interferogram can be subjected to the next step of conjugate multiplication and interference processing.

Elimination of the flat ground effect: the flat ground effect refers to the periodic changes of the interferogram fringes in the azimuth and distance directions when characterizing the flat terrain, which cannot reflect the real topographic changes. Therefore, eliminating the flat-earth effect is an important step before the phase unwrapping operation.

Interference filtering processing: the unfiltered interferogram usually has a lot of noise. If the phase unwrapping is performed directly, it will lead to a large deviation in the result. Before unwrapping, the interferogram needs to be filtered. The filtering methods include spatial filtering method and filtering method based on wavelet transform.

Phase unwrapping: phase unwrapping is the process of restoring the interference phase after the flat ground effect has been eliminated from $(-\pi, \pi)$ to the real phase, so that the interference phase corresponds to the terrain elevation, and the result of phase unwrapping will directly affect the to the accuracy of the digital elevation reconstruction.

DEM reconstruction: after the real phase is obtained through phase unwrapping, the digital elevation model can be reconstructed according to the InSAR elevation measurement principle introduced in this chapter in combination with orbital parameters.

3.2. The Basic Theory of GAN. In GAN, the basic architecture of both the generator and the discriminator are neural networks. The input of the generation network is a random noise vector that conforms to a certain distribution, the output is generally a random image, and the input of the discriminator is a real image from the data set or an image generated by the generator and the discriminator. When GAN is training, the generator and the discriminator will alternately train, and the samples generated by the generator will be transformed according to the output of the discriminator during the training process. Therefore, the optimization objective function of GAN is shown in the following formula:

$$\mathscr{L}_{\mathrm{GAN}}(G, D) = \mathbb{E}_{\mathrm{x}}[\lg D(x)] + \mathbb{E}_{z}[\lg (1 - D(G(z)))], \quad (6)$$

where x represents the random noise vector input to the generator, z is the output of the generator, G represents the generator network, and D represents the discriminator network. The generation countermeasure network (GAN) has two networks, a generator network and a discriminator network. These two networks can be neural networks, from convolutional neural networks, recursive neural networks to automatic encoders. In this configuration, the two networks participate in the competitive game and try to surpass each other while helping them complete their tasks. In the original GAN, the architectures of both the generator network and the discriminator network are multilayer perceptrons, so the generation ability of the generator and the discriminative ability of the discriminator are greatly limited. In DCGAN, the authors used convolutional neural network as the basic architecture of generator and discriminator to enhance the generative and discriminative capabilities of GAN. At the same time, in order to make it differentiable in network training, DCGAN removes the pooling layer in the general CNN and replaces the fully connected layer of the discriminant network with a global pooling layer to reduce the amount of computation.

3.2.1. GAN Optimization and Generation Control. Although DCGAN improves the generation ability and discrimination ability of GAN, it does not fundamentally solve the problems of GAN training difficulties, unstable generator training, and lack of diversity of generated samples during the training process. Wasserstein Generative Adversarial Network (Wasserstein GAN, WGAN) fundamentally analyzed these existing problems and gave a series of solutions. WGAN analyzes the reasons for the problems of the original GAN, mainly including the following points: (1) the better the discriminator, the more serious the generator gradient disappears; (2) the original generator loss function is unreasonable, and the generator loss is minimized during training When the operation is performed, it is equivalent to minimizing an unreasonable measurement distance between the generated sample and the target. Doing this leads to two problems: (1) unstable gradients and (2) insufficient generative diversity for the generator. At the same time, WGAN also provides a series of solutions: (1) remove the sigmoid activation function of the last layer of the discriminator; (2) do not perform logarithmic transformation when calculating the loss functions of the generator and discriminator; (3) each time after updating the parameters of the discriminator, truncate their absolute values to be less than or equal

to a fixed constant; (4) do not use momentum-based optimization algorithms (including momentum and Adam) in GAN training. It is recommended to use RMSProp, SGD, and other excellent primitives. The GAN not only has the above-mentioned problems, but the most important thing is that the generation results of the generator are not controllable. The main reason is that the input of the generator is a random noise vector, so the output of the generator will completely depend on the input random noise vector, making the output of the generator unpredictable. cGAN controls the generation results of the generator by adding generative and discriminative conditions. Compared with the original GAN model, the optimization objective function of cGAN is shown in formula (7), where y is the added constraint vector.

$$\mathscr{L}_{\mathrm{cGAN}}(G, D) = \mathbb{E}_{\mathrm{x}}[\lg D(x|y)] + \mathbb{E}_{\mathrm{z}}[\lg (1 - D(G(z|y)))]. \quad (7)$$

3.2.2. The Loss Function Mechanism of GAN. The main function of the discriminator network in GAN is to guide the training of the generator by judging the authenticity of the input samples, so that the output of the generator is closer to the real samples. Specifically, the role of the discriminator is equivalent to first extracting the features of the generated samples or real samples and then discriminating the gap between the generated samples and the real samples at the feature level. The general supervised learning network will use a predefined loss function to calculate the error between the output of the model and the real sample, so as to guide the training of the model. Therefore, the discriminative mechanism of GAN is equivalent to providing a trainable loss function to supervise the training of the generator. Figure 2 is a graph of the GAN loss function. If the generative network structure is replaced by an end-to-end segmentation model structure, GAN is quite a more powerful segmentation model at this time, because it has a better trainable loss function. The pix model perfectly solves the image translation problem by applying the cGAN mechanism for the first time. The cGAN optimization objective function of Pix2pix is shown in the following formula (8):

$$\mathscr{L}_{\mathrm{cGAN}}(G, D) = \mathbb{E}_{\mathrm{x,y}}[\lg D(x, y)] + \mathbb{E}_{\mathrm{x,z}}[\lg (1 - D(x, G(x, z)))]. \quad (8)$$

In Pix2pix, the input x of the generator is changed from a random vector to an image, and the input of the discriminator is the original input image x spliced in the original generated image z or marked image y as a condition for discrimination. Inspired by the work of Pix2pix, this paper constructs different GAN-based segmentation models in different medical image segmentation tasks and achieves very good segmentation results.

3.3. Research on Traditional Phase Unwrapping Algorithms

3.3.1. Phase Unwrapping Algorithms. Based on path tracking, the concept of residue point in 1988 and proposed the classical branch-cut method for phase unwrapping (BranchCutsPhaseUnwrapping, BCPU). The algorithm generates

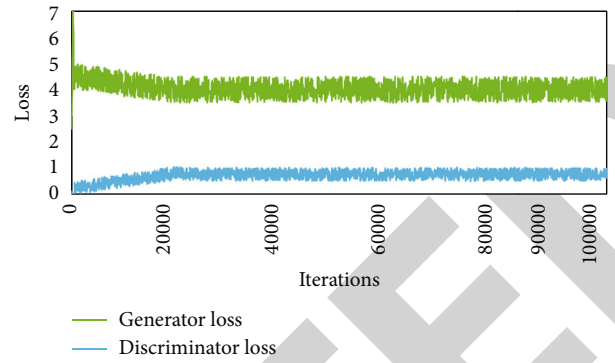

Figure 2: GAN loss function graph.

branch tangents by identifying positive and negative residue points. According to the principle that the integral path does not cross the branch tangents, the error transmission caused by unwrapping of discontinuous points is avoided. The definition of the residual point is as follows: calculate the adjacent phase gradient winding value, as follows:

$$\begin{aligned} \Delta_1 &= W[\psi(m+1, n) - \psi(m, n)], \\ \Delta_2 &= W[\psi(m+1, n+1) - \psi(m+1, n)], \\ \Delta_3 &= W[\psi(m, n+1) - \psi(m+1, n+1)], \\ \Delta_4 &= W[\psi(m, n) - \psi(m, n+1)]. \end{aligned} \quad (9)$$

Adding the above formula can get

$$S = \sum_{i=1}^{4} \Delta_i. \quad (10)$$

If s is greater than 0, that is, the polarity of the residual point charge is "positive," it means that the pixel $\Psi(m, n)$ in the upper left corner of the closed path is a positive residual point, otherwise, $\psi(m, n)$ is called a negative residual point. Count the points.

3.3.2. Quality Graph Guidance Algorithm. In addition to the above-mentioned method of determining the integral path using the residual point distribution, other auxiliary information can also be used to plan the integral path. The QualityGuidePhaseUnwrapping algorithm (QGPU) analyzes the phase quality, so that the winding phase is unwrapped in the direction of high-quality pixels to low-quality pixels. The core of the mass map-guided method is to use the phase quality of the interferogram to guide the interferometric pixels for diffusion. The following are the algorithm steps:

Step 1. Take the pixel with the highest quality in the winding interferogram as the starting point of unwrapping, mark it as the unwrapped pixel, and store the adjacent pixels around the starting pixel in the adjacency list.

Step 2. Sort the pixels in the adjacency list according to the quality value, select the pixel with the highest quality, mark the pixel as the unwrapped point, remove the unwrapped

pixel from the adjacency list, and then, put this pixel. The adjacent unwrapped pixels are stored in the adjacency list.

Step 3. Repeatedly select the pixel with the highest quality in the adjacency list to perform Step 2, until the unwrapped pixels in the adjacency list are empty, and the phase unwrapping is completed.

The mass map-guided algorithm references the mass map as auxiliary information to avoid error propagation due to unwrapping discontinuous phases. In the case of a relatively reliable phase quality map, the unwrapping effect of the algorithm is better than that of the Goldstein branch-cut method. Otherwise, the unwrapping results may be inaccurate due to the existence of unbalanced residual points. In this paper, we use weighting to avoid the error caused by residual points, which leads to the accumulation and propagation of errors. The residual points and nonresidual points can be distinguished by solving the quality map of the wrapped phase, so as to obtain better expansion results. At present, there are mainly four methods to evaluate the quality of interferograms: coherence coefficient map, pseudocoherence map, phase derivative change map, and maximum phase gradient map.

(1) The coherence coefficient map is defined as follows:

$$\gamma = \frac{\lim_{M,N\longrightarrow\infty}\sum_{n=1}^{N}\sum_{m=1}^{M}|\mu_1(n,m)||\mu_2(n,m)|}{\sqrt{\lim_{M,N\longrightarrow\infty}\sum_{n=1}^{N}\sum_{m=1}^{M}|\mu_1(n,m)|^2\lim_{M,N\longrightarrow\infty}\sum_{n=1}^{N}\sum_{m=1}^{M}|\mu_2(n,m)|^2}} \tag{11}$$

In the formula, Y is the coherence coefficient value; M and N are the data size for calculating the coherence; m and n are the row and column numbers in the data.

(2) The pseudocoherence coefficient map is defined as follows:

$$Z_{m,n} = \frac{\sqrt{\left(\sum\cos\phi_{i,j}\right)^2 + \left(\sum\sin\phi_{i,j}\right)^2}}{k^2} \tag{12}$$

(3) The phase derivative change diagram is defined as follows:

$$Z_{m,n} = \frac{\sqrt{\sum\left(\Delta_{m,n}^{x} - \bar{\Delta}_{m,n}^{x}\right)^2} + \sqrt{\sum\left(\Delta_{m,n}^{y} - \bar{\Delta}_{m,n}^{y}\right)^2}}{k^2} \tag{13}$$

(4) The maximum phase gradient map is defined as follows:

$$Z_{m,n} = \begin{cases} \max\left[\left|\Delta_{m,n}^{x}\right|\right] \\ \max\left[\left|\Delta_{m,n}^{y}\right|\right] \end{cases} \tag{14}$$

In the above four evaluation methods, the coherence coefficient map indicates the quality of the corresponding position of the interference image through the brightness and darkness, so this is the most intuitive interference phase quality evaluation standard. When the terrain is relatively flat and the phase change is not obvious, the pseudocoherence coefficient map is often used. Similar to the maximum phase gradient, it also appears as low-quality data in areas with steep changes in terrain, which is not conducive to guiding the unwrapping path. In the case where the coherence map cannot be obtained, the effect of the phase derivative change map is relatively more reliable.

3.4. Phase Unwrapping Algorithm Based on Deep Learning

3.4.1. Phase Unwrapping Network Based on FC-DenseNet. According to this network, the excellent performance on the data set confirms the potential of this network in dealing with semantic segmentation problems. Traditional neural networks such as LeNet, VGGNet, FC-DenseNet can reuse the feature information of each layer through dense block (DB) with its unique multilayer cascade structure, and the input of each layer of network includes all previous layer learning The obtained image features can improve the utilization rate of feature information by the network. In order to deal with the complex phase unwrapping problem, this paper deepens the network on the basis of the original model and proposes a phase unwrapping model based on FC-DenseNet. The schematic diagram of the network model is as follows. As shown in Figure 3, (a) is the initial model, and (b) is the deepened model.

It can be seen from Figure 3 that the structure of the deepened FC-DenseNet model is similar to that of U-net, with the downsampling path on (a) and the upsampling path on (b). The network is composed of two convolution layers, nine dense blocks, two transition layers, layers and jump connections. In the phase unwrapping model based on the FC-DenseNet network, the black arrow represents the flow direction of the network, the blue box represents the convolution module (convolutional layer + batch normalization BN + activation function ReLu + Dropout layer); TD is denoted as the downsampling transition layer; TU is denoted as the upsampling transition layer; and the gray arrows are skip connections. The higher resolution information in the encoding path is passed to the decoding path through skip connections. From the input layer, the current output is concatenated into the input of the next layer. If the operation is repeated four times, the final dense block output is the concatenation result of the output features of the four convolutional layers. Therefore, such a multilayer dense structure combines the feature information contained in the remaining layers to ensure the efficient use of information.

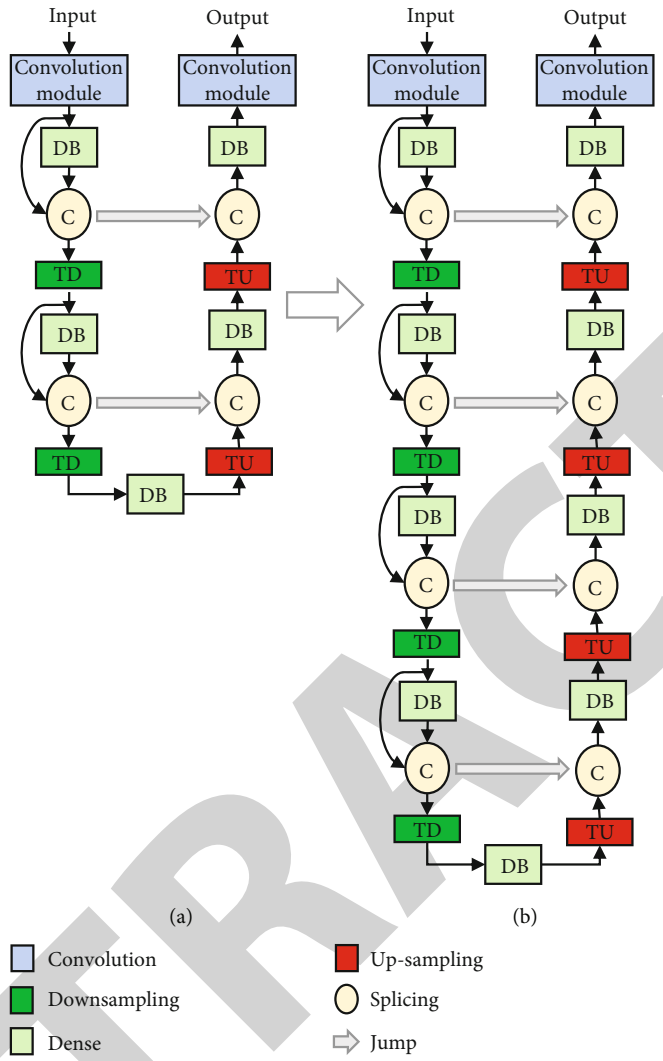

Figure 3: Initial model and phase unwrapping model based on FC-DenseNet network.

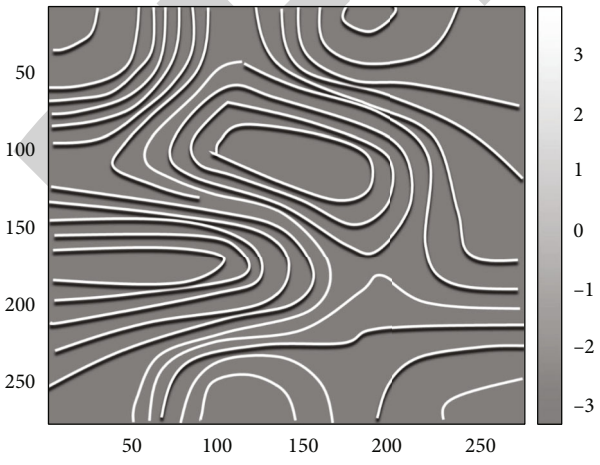

Figure 4: Noise winding phase diagram.

4. Result Analysis and Discussion

4.1. Experimental Analysis of Simulated Interferograms. Interferogram denoising is a key step in InSAR data processing. If the noise pollution in the interferogram is serious. This section will use simulated and measured interferometric maps to analyze the branch-cut method, quality map-guided method, FFT-based least squares method (LSPU), and iterative least squares method (ILSPU) introduced in this chapter. Based on the unscented Kalman filter algorithm (UKFPU), five classical phase unwrapping algorithms are tested, respectively, and the performance of each algorithm is analyzed by comparing the unwrapping results of each algorithm. The unit of horizontal and vertical coordinates in the figure is pixels, and the unit of the color label on the right is radians.

(1) Simulation experiment 1: Figure 4 shows the simulated terrain winding interferogram (signal-to-noise ratio is 8 dB). The phase unwrapping of Figure 4 is carried out using the branch-cut method, the quality

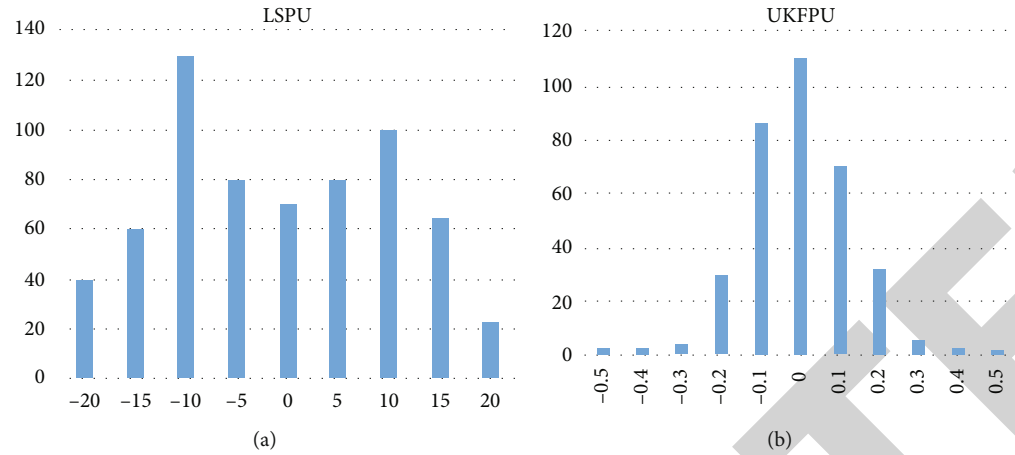

Figure 5: The statistical histogram of the unwrapping error of each algorithm: (a) LSPU algorithm; (b) UKFPU algorithm.

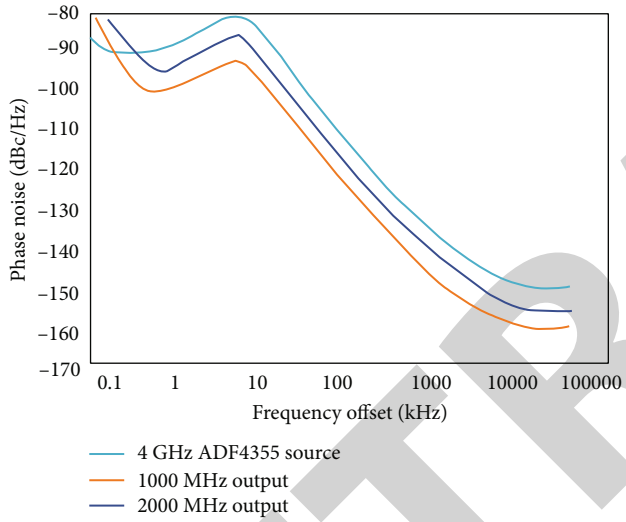

Figure 6: Interferogram segmentation results after adding noise.

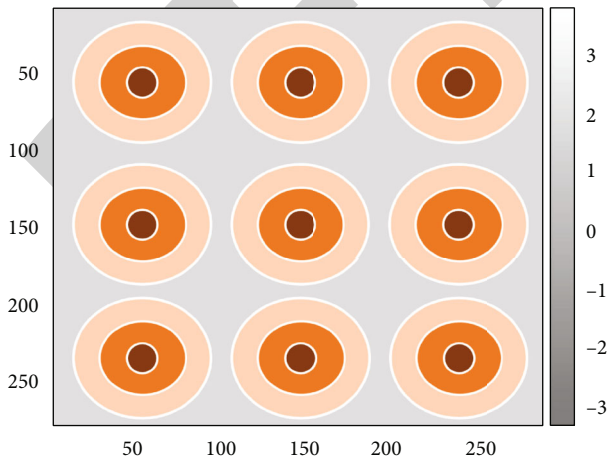

Figure 7: Noise winding interference diagram.

map-guided method, LSPU, ILSPU, and UKFPU, respectively, and the unwrapping results of each algorithm are shown in Figure 4

It can be clearly seen from Figure 5 that the unwrapping results of the LSPU algorithm have a large error, and the error values are distributed between -20 and 20, while the unwrapping errors of the other four algorithms are mostly distributed between -1 and +1. The experimental results show that other algorithms except the LSPU algorithm have good unwrapping effect when dealing with interferograms with high signal-to-noise ratio.

(2) Simulation experiment 2: Figure 6 shows the interferogram with added noise. It can be seen from the figure that when dealing with interferograms with lower signal-to-noise ratios. Too many points are left in the noisy area, which leads to the "islanding" effect, and a large number of unwrapped black spots appear in the unwrapped result, which cannot effectively unwrap all the interferograms. The unwrapping error is mainly distributed around 0, but there are still areas in the unwrapping result that are inconsistent with the original real phase map

(3) Simulation experiment 3: Figure 7 is the interferogram of winding. In order to compare the unwrapping efficiency of each algorithm and the unwrapping accuracy under different signal-to-noise ratios, different degrees of noise are added to Figure 7 before unwrapping. Since the statistical standard of the branch-cut method is different from other algorithms, the statistics and analysis are not carried out in this experiment. As the signal-to-noise ratio of the interferogram gradually decreases, the mean square error of the unwrapping results of each algorithm is also increasing

Figure 7 shows the distribution of residual points of the measured optical interferogram. From the unwrapping results of the measured terrain, it can be seen that when the branch tangent method unwrapped the dense area of the residual points of the interferogram, the branch tangent

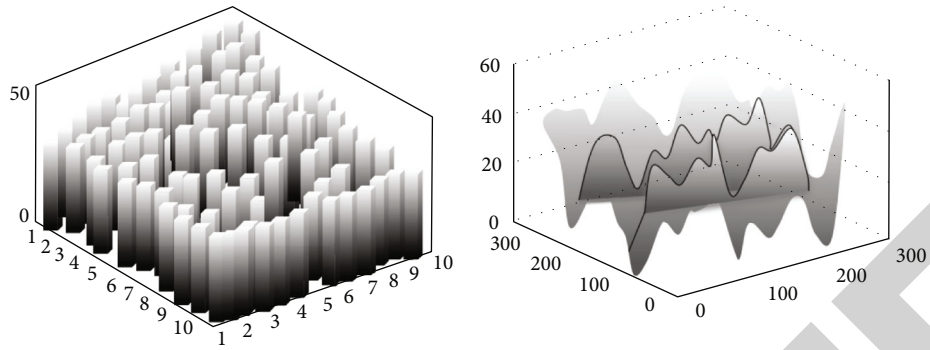

(a) Create random matrix (b) Interpolation zoom

Figure 8: A simulated InSAR data set.

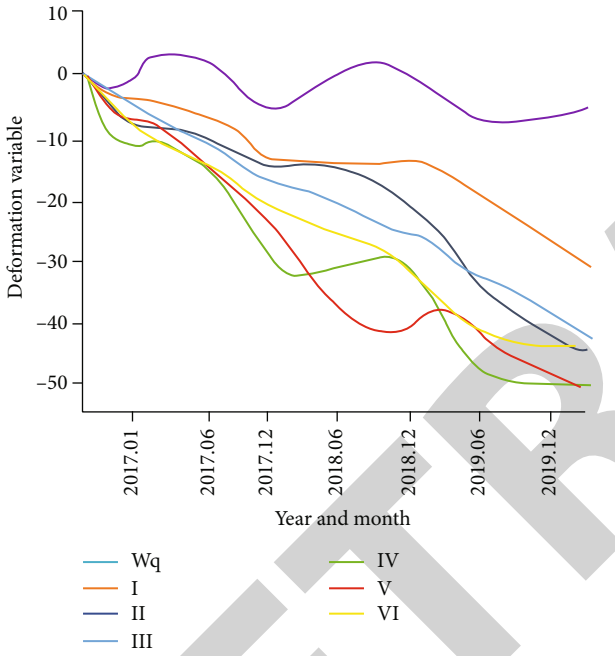

Figure 9: Phase unwrapping feature points obtained by the correlation coefficient method.

lines formed a closed loop, and the complete interferogram cannot be unwrapped; the unwrapped result of the mass-map guided method is basically consistent with the real phase, but it can be seen from the rewinding image that there are still unresolved edges of the interference fringes. For filtering noise, the fringe distortion in unwrapped phase rewind images of LSPU and ILSPU is not obvious, and there is burr noise, indicating that although the minimum norm class algorithm has relatively high phase unwrapping efficiency, it is easy to perform in the unwrapping process. The details of the interferogram are ignored, causing the unwrapped results to deviate too much from the true phase.

4.2. Research on GAN-Based Deep Learning Phase Unwrapping Algorithm

4.2.1. InSAR Interferogram Data Set. Construction of data set is an important step in supervised learning, and high-quality data sets can often improve the quality of network model training and the accuracy of prediction. Data sets with better quality often have the following two characteristics:

(1) The amount of sample data is moderate. If the amount of data is too large, the neural network will lead to overfitting after generalizing a large amount of data, and if the amount of data is too small, it will lead to underfitting. Therefore, in the actual training process, data enhancement is generally adopted to expand the data

(2) The sample data types are diverse. If the sample data features are single, the trained network has poor robustness and weak generalization ability, and the data set with diverse features is more representative. In the confrontation training (as a classical algorithm to improve the robustness of the model), the author effectively combines it with the training process of GAN, and names it as the combination model rob GAN. Experiments show that rob GAN can not only make the training of GAN more stable and the generation results more realistic but also reduce the performance gap between the training set and the test set. Currently, there are no publicly available InSAR data sets in the field of deep learning phase unwrapping. In this paper, the simulated InSAR data, quasimeasured InSAR data, and DEM terrain data of 256 pixels × 256 pixels are constructed, respectively, and the three types of data are mixed to form a complete InSAR data set. Label units are radians. In phase unwrapping, the relationship between the real phase φ and the corresponding wrapping phase φ can be expressed as

$$\varphi = \text{angle}[\exp(j\phi)]. \tag{15}$$

Among them, the winding phase $\varphi \in (-\pi, +n)$. When creating an InSAR data set, first generate the real phase value of InSAR, calculate the winding interferogram through the above formula, and construct a simulated InSAR data set as shown in Figure 8. Columns in Figure 8(a) are the

randomly created 10×10 initial matrices; Figure 8(b) is the interpolation and enlargement of the original initial matrix; in the network training process, the real phase map generated above is used as its corresponding noise label image of the wrapped phase map.

Figure 9 is a phase unwrapping feature point diagram obtained by the correlation coefficient method. The larger the correlation coefficient, the smaller the interference and the better the reliability; the smaller the correlation coefficient, the greater the interference, and the worse the reliability. Therefore, when the unit phase unwrapping is performed, the area with the largest average correlation coefficient is selected as the object of the network planning algorithm, and the remaining three areas in the unit are used as the unwrapping object of the FFT-based least squares algorithm. Similarly, in the process of image correction and fusion, the area with the largest average correlation coefficient should be used as the benchmark for correction and fusion.

5. Conclusion

This paper applies the deep learning method to phase unwrapping to expand and explore the potential of GAN neural network in the field of InSAR interferogram phase unwrapping. The main research work is as follows: the InSAR data set for deep learning phase unwrapping is proposed. The mixture of simulated data and quasimeasured data improves the diversity of sample data features in the training set and increases the generalization ability of the neural network. The experimental results show that although the structure level is deep enough, the FC Dense Net network model cannot process interferograms with low SNR and complex interference fringes. The experimental results of simulated and measured terrain interferometric unwrapping show that, compared with other types of deep learning phase unwrapping methods, the proposed method achieves better results in both simulated and measured data unwrapping experiments, with a relatively small mean square error and a better solution. The winding precision is relatively high, and the noise resistance is relatively strong. This paper has some limitations. When the interference filtering of the original interferogram suppresses a lot of noise, it will also lead to the loss of a lot of useful information. The irregular window needs further research and analysis. The research also needs to improve the ability of adaptive median filter to remove phase particle noise and keep it unclear.

Data Availability

The data used to support the findings of this study are available from the corresponding author upon request.

Conflicts of Interest

The authors declare that they have no known competing financial interests or personal relationships that could have appeared to influence the work reported in this paper.

References

[1] K. D. Murray, R. B. Lohman, and D. Bekaert, "Cluster-based empirical tropospheric corrections applied to InSAR time series analysis," *IEEE Transactions on Geoscience and Remote Sensing*, vol. 3, no. 99, pp. 1–9, 2020.

[2] L. Pulvirenti, M. Chini, and N. Pierdicca, "InSAR multitemporal data over persistent scatterers to detect floodwater in urban areas: a case study in Beletweyne, Somalia," *Remote Sensing*, vol. 13, no. 1, p. 37, 2020.

[3] Z. Yuan, Z. Lu, L. Chen, and X. Xing, "A closed-form robust cluster-analysis-based multibaseline InSAR phase unwrapping and filtering algorithm with optimal baseline combination analysis," *IEEE Transactions on Geoscience and Remote Sensing*, vol. 58, no. 6, pp. 4251–4262, 2020.

[4] M. Wang, H. Lu, S. Liu, and Z. Zhu, "How to mislead AI-assisted network automation in SD-IPoEONs: a comparison study of DRL- and GAN-based approaches," *Journal of Lightwave Technology*, vol. 38, no. 20, pp. 5574–5585, 2020.

[5] K. S. Gill, S. Nguyen, and M. Thein, "Three-way deep neural network for radio frequency map generation and source localization," 2021, https://arxiv.org/abs/2111.12175.

[6] K. B. Park, S. H. Choi, and J. Y. Lee, "M-GAN: retinal blood vessel segmentation by balancing losses through stacked deep fully convolutional networks," *IEEE Access*, vol. 8, no. 99, pp. 146308–146322, 2020.

[7] X. Y. Lim, K. B. Gan, and N. A. A. Aziz, "Deep ConvLSTM network with dataset resampling for upper body activity recognition using minimal number of IMU sensors," *Applied Sciences*, vol. 11, no. 8, p. 3543, 2021.

[8] S. Krylov and V. Krylov, "Inverse problem solving approach using deep network trained by GAN simulated data," *Journal of Physics: Conference Series*, vol. 2021, no. 1, article 012002, 12 pages, 2021.

[9] A. Amyar, S. Ruan, P. Vera, P. Decazes, and R. Modzelewski, "RADIOGAN: deep convolutional conditional generative adversarial network to generate PET images," 2020, https://arxiv.org/abs/2003.08663.

[10] A. Kumar, A. Alsadoon, P. W. C. Prasad et al., "Generative adversarial network (GAN) and enhanced root mean square error (ERMSE): deep learning for stock price movement prediction," *Papers*, vol. 17, no. 20, pp. 115–123, 2021.

[11] R. Nandhini Abirami, P. M. Durai Raj Vincent, K. Srinivasan, U. Tariq, and C. Y. Chang, "Deep CNN and deep GAN in computational visual perception-driven image analysis," *Complexity*, vol. 2021, no. 25, Article ID 5541134, 30 pages, 2021.

[12] T. W. Tang, W. H. Kuo, J. H. Lan, C. F. Ding, H. Hsu, and H. T. Young, "Anomaly detection neural network with dual auto-encoders GAN and its industrial inspection applications," *Sensors*, vol. 20, no. 12, 2020.

[13] N. Shivsharan and S. Ganorkar, "Diabetic retinopathy detection using optimization assisted deep learning model: outlook on improved grey wolf algorithm," *International Journal of Image and Graphics*, vol. 21, no. 3, article 2150035, 2021.

[14] Y. Hua, R. Li, Z. Zhao, X. Chen, and H. Zhang, "GAN-powered deep distributional reinforcement learning for resource management in network slicing," *IEEE Journal on Selected Areas in Communications*, vol. 38, no. 2, pp. 334–349, 2020.

[15] R. Li, X. Lv, J. Yuan, and J. Yao, "A triangle-oriented spatial–temporal phase unwrapping algorithm based on irrotational constraints for time-series InSAR," *IEEE Transactions on*

Geoscience and Remote Sensing, vol. 57, no. 12, pp. 10263–10275, 2019.

[16] Y. Ma and Y. Li, "Millimeter-wave InSAR target recognition with deep convolutional neural network," *IEICE Transactions on Information and Systems*, vol. E102.D, no. 3, pp. 655–658, 2019.

[17] D. Chai, S. Newsam, H. K. Zhang, Y. Qiu, and J. Huang, "Cloud and cloud shadow detection in Landsat imagery based on deep convolutional neural networks," *Remote Sensing of Environment*, vol. 225, no. 5, pp. 307–316, 2020.

[18] S. Ye, L. Xu, and X. Li, "Vehicle-mounted self-organizing network routing algorithm based on deep reinforcement learning," *Wireless Communications and Mobile Computing*, vol. 2021, no. 11, Article ID 9934585, 9 pages, 2021.

[19] S. Xu and Y. Jiang, "Research on trajectory tracking method of redundant manipulator based onPSO algorithm optimization," *Computer Modeling in Engineering and Science*, vol. 9, no. 1, pp. 18–22, 2020.

[20] J. Liang, P. Chen, and M. Wu, "Research on an image denoising algorithm based on deep network learning," *Journal of Physics: Conference Series*, vol. 2021, no. 3, article 032112, 8 pages, 2021.